Modelling and modal properties of nuclear fuel assembly

V. Zeman[a,*], Z. Hlaváč[a]

[a]*Faculty of Applied Sciences, University of West Bohemia, Univerzitní 22, 306 14 Plzeň, Czech Republic*

Abstract

The paper deals with the modelling and modal analysis of the hexagonal type nuclear fuel assembly. This very complicated mechanical system is created from the many beam type components shaped into spacer grids. The cyclic and central symmetry of the fuel rod package and load-bearing skeleton is advantageous for the fuel assembly decomposition into six identical revolved fuel rod segments, centre tube and skeleton linked by several spacer grids in horizontal planes. The derived mathematical model is used for the modal analysis of the Russian TVSA-T fuel assembly and validated in terms of experimentally determined natural frequencies, modes and static deformations caused by lateral force and torsional couple of forces. The presented model is the first necessary step for modelling of the nuclear fuel assembly vibration caused by different sources of excitation during the nuclear reactor VVER type operation.

© 2011 University of West Bohemia. All rights reserved.

Keywords: fuel assembly, modelling of vibration, modal values, decomposition method

1. Introduction

Nuclear fuel assemblies are in term of mechanics very complicated system of beam type, which basic structure is formed from large number of parallel identical fuel rods, some guide thimbles and centre tube, which are linked by transverse spacer grids to each other and with skeleton construction [8]. The spacer grids are placed on several horizontal level spacings between support plates in reactor core [9].

Dynamic properties of nuclear fuel assembly (FA) are usually investigated using global models, whose properties are gained experimentally [4, 7]. Eigenfrequencies and eigenvectors, investigated by measurement in the air, serve as initial data for parametric identification of the FA global model considered as one dimensional continuum of beam type [2]. This consideration is acceptable for a mathematical modelling and computer simulation of the whole nuclear reactor vibration caused by seismic excitation [2] and pressure pulsations [10] in terms of FA skeleton deformation. These global models of FA do not enable investigation of dynamic deformations and load of FA components and abrasion of fuel rods coating [5].

The goal of the paper is a development of analytical method for modelling and analysis of the FA modal properties. Motivation of this research work was exchange the American nuclear VVANTAGE 6 FA for Russian TVSA-T FA in NPP Temelín. The newly developed conservative mathematical model and corresponding computer model of the hexagonal type nuclear FA in parametric form enables to analyse modal properties, sensitivity to FA design parameters and parametric identification of FA components on the basis of measured static deformations, eigenfrequencies and eigenvectors. The presented methodology and FA detailed model is the

*Corresponding author. Tel.: +420 377 632 332, e-mail: zemanv@kme.zcu.cz.

first necessary step to modelling the dynamic response caused by forced and kinematics excitation. Dynamic forces between fuel rods and spacer grids will be used for calculation of expected lifetime period of nuclear FA in term of abrasion of fuel rods coating and fatigue live.

2. Mathematical models of FA subsystems

In order to model the fuel assembly, the system is divided into subsystems — identical rod segments (S), centre tube (CT) and load-bearing skeleton (LS) fixed in bottom part in lower piece (Fig. 1).
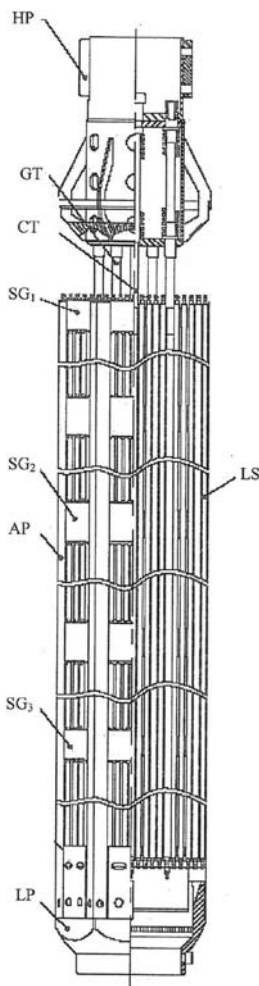

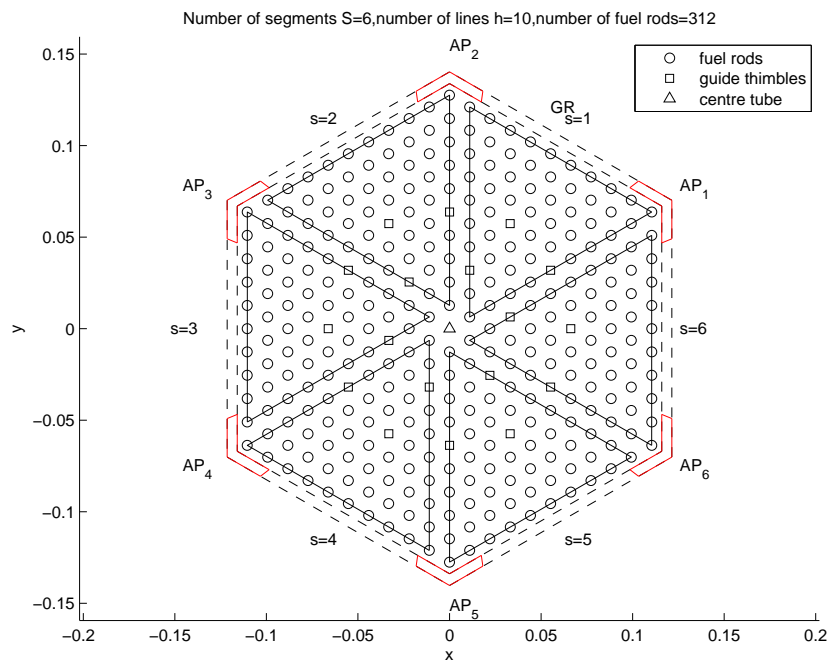Fig. 1. Scheme of the fuel assembly

Fig. 2. The FA cross-section

2.1. Model of the rod segment

Because of the cyclic and central symmetric package of fuel rods and guide thimbles with respect to centre tube (Fig. 2), the FA decomposition of the identical rod segment $s = 1, \ldots, S$ (on the Fig. 2 for $S = 6$) shall be applied. Each rod segment is composed of R fuel rods with fixed bottom ends in lower piece and guide thimbles (GT) fully restrained in lower and head pieces. The fuel rods and guide thimbles inside the segments are linked by transverse spacer grids of three types ($\mathrm{SG}_1 - \mathrm{SG}_3$) which elastic properties are expressed by linear springs placed
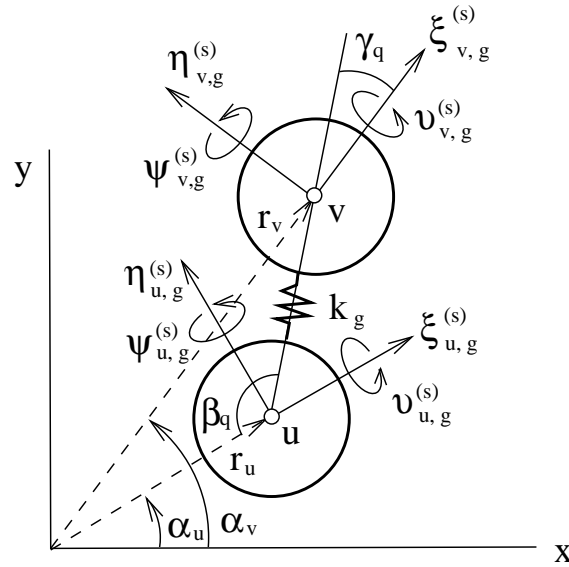
Fig. 3. The spring between two rods replacing the stiffness of spacer grid g

on several level spacings $g = 1, \ldots, G$ (see Fig. 1).The fuel rods are embedded into spacer grids with small initial tension, which wouldn't fall below zero during core operation.

The mathematical model of the rod segments isolated from adjacent segments (without linkages between segments) was derived [11] in the special coordinate system

$$\boldsymbol{q}_s = [\boldsymbol{q}_{1,s}^T, \ldots, \boldsymbol{q}_{r,s}^T, \ldots, \boldsymbol{q}_{R,s}^T]^T \,, \tag{1}$$

where $\boldsymbol{q}_{r,s}$ is vector of nodal point displacements of one rod r (fuel rod or guide thimble) on the level of all spacer grids g in the form

$$\boldsymbol{q}_{r,s} = [\ldots, \xi_{r,g}^{(s)}, \eta_{r,g}^{(s)}, \vartheta_{r,g}^{(s)}, \psi_{r,g}^{(s)}, \ldots]^T \,, \ g = 1, \ldots, G \,. \tag{2}$$

Lateral displacements $\xi_{r,g}^{(s)}$, $\eta_{r,g}^{(s)}$ in contact nodal points with spacer grid g are mutually perpendicular whereas displacements $\xi_{r,g}^{(s)}$ are radial with respect to vertical central axis of FA. Displacements $\vartheta_{r,g}^{(s)}$, $\psi_{r,g}^{(s)}$ are bending angles of rod cross-section around lateral axes in contact nodal points (see Fig. 3).

The conservative mathematical model of the arbitrary isolated rod segment s was derived on the basis of Rayleigh beam theory in the form [11]

$$\boldsymbol{M}_S \ddot{\boldsymbol{q}}_s + \left(\boldsymbol{K}_S + \sum_{q=1}^{Q} \sum_{g=1}^{G} \boldsymbol{K}_{q,g} \right) \boldsymbol{q}_s = \boldsymbol{0} \,, \ s = 1, \ldots, S \,, \tag{3}$$

where Q is the number of the transverse linear springs of one spacer grid inside one segment and $\boldsymbol{K}_{q,g}$ is stiffness matrix corresponding to the coupling q by means of the spring k_g on the level of spacer grid g between two fuel rods u and v of the segment s. These coupling stiffnesses are determined by polar coordinates r_u, α_u and r_v, α_v of the linked fuel rods [3] and nonzero elements are localized at positions corresponding to displacements $\xi_{u,g}^{(s)}$, $\eta_{u,g}^{(s)}$, $\xi_{v,g}^{(s)}$, $\eta_{v,g}^{(s)}$ in the vector of generalized coordinates $\boldsymbol{q}_s$ in (1). The mass $\boldsymbol{M}_s$ and stiffness $\boldsymbol{K}_s$ matrices of the fuel rods and guide thimbles in one segment are block diagonal and have the form

$$\boldsymbol{X}_s = \mathrm{diag}[\boldsymbol{X}_R, \ldots, \boldsymbol{X}_{GT}, \ldots, \boldsymbol{X}_R] \in R^{4GR}, \ \boldsymbol{X} = \boldsymbol{M}, \boldsymbol{K} \,, \tag{4}$$

whereas matrices $\boldsymbol{X}_R\left(\boldsymbol{X}_{GT}\right)$ correspond to one mutually uncoupled fuel rod (guide thimble). All fuel rods and guide thimbles are parallel and have identical boundary conditions (fuel rods have fixed lower ends and guide thimbles are fully restrained).

2.2. Model of the centre tube

The fully restrained centre tube (see Fig. 1 and Fig. 2) is discretized into G nodal points on the level of spacer grids $g = 1, \ldots, G$ by means of $G + 1$ prismatic beam finite elements [6] in the coordinate system

$$\boldsymbol{q}_{CT} = [\ldots, x_g, y_g, \vartheta_g, \psi_g, \ldots]^T, \, g = 1, \ldots, G, \tag{5}$$

where lateral displacements x_g, y_g are oriented into axes x, y (Fig. 3). Mass and stiffness matrices $\boldsymbol{M}_{CT}$, $\boldsymbol{K}_{CT}$ are symmetric of order $4G$.

2.3. Model of load-bearing skeleton

The load-bearing skeleton (further only skeleton) is created of S (on the Fig. 2 for $S = 6$) angle pieces (AP) coupled by divided grid rim (GR) at all levels of spacer grids (Fig. 4). Each angle piece with fixed bottom ends in lower piece is discretized into nodal points C_g in cross-section centre of gravity on the level of spacer grids $g = 1, \ldots, G$. The mathematical model of the skeleton without of couplings with spacer grids is derived in the coordinate system

$$\boldsymbol{q}_{LS} = [\boldsymbol{q}_{AP_1}^T, \ldots, \boldsymbol{q}_{AP_s}^T, \ldots, \boldsymbol{q}_{AP_S}^T]^T, \tag{6}$$

where $\boldsymbol{q}_{AP_s}$ is vector of nodal points displacements for particular angle piece s on the level of all grid rim g in the form

$$\boldsymbol{q}_{AP_s} = [\ldots, \xi_{AP,g}^{(s)}, \eta_{AP,g}^{(s)}, \varphi_{AP,g}^{(s)}, \vartheta_{AP,g}^{(s)}, \psi_{AP,g}^{(s)}, \ldots]^T, \, g = 1, \ldots, G. \tag{7}$$

Lateral displacements $\xi_{AP,g}^{(s)}$, $\eta_{AP,g}^{(s)}$ of cross-section centre of gravity on the level of spacer grid g are mutually perpendicular whereas displacement $\xi_{AP,g}^{(s)}$ is radial (see Fig. 4). Displacements $\varphi_{AP,g}^{(s)}$, $\vartheta_{AP,g}^{(s)}$, $\psi_{AP,g}^{(s)}$ are torsional and bending angles of angle piece cross-section around vertical and lateral axes (in Fig. 4 indexes are let-out).
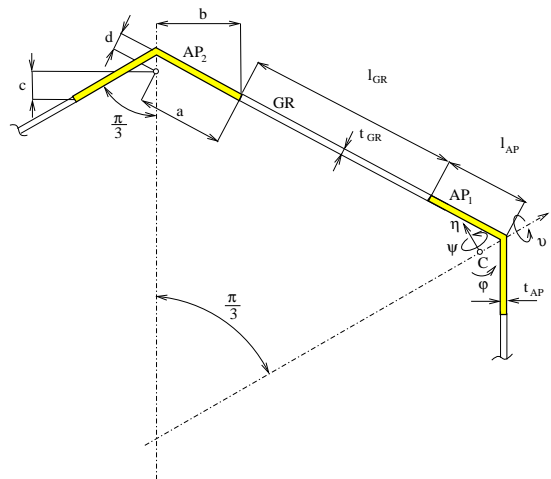

Fig. 4. Scheme of the load-bearing skeleton (part)

Mathematical model of the angle piece beam element between nodal points C_{g-1} and C_g in alternate coordinate system (indexes AP and (s) of coordinates are let-out)

$$\boldsymbol{q}_{AP}^{(e)} = [\xi_{g-1}, \psi_{g-1}, \xi_g, \psi_g, \eta_{g-1}, \vartheta_{g-1}, \eta_g, \vartheta_g, \varphi_{g-1}, \varphi_g]^T \tag{8}$$

is written by mass and stiffness matrices in the form [1]

$$\boldsymbol{M}_{AP}^{(e)} = \rho \begin{bmatrix} \boldsymbol{S}_1^{-T}(A\boldsymbol{I}_\phi + J_\eta \boldsymbol{I}_{\phi'})\boldsymbol{S}_1^{-1} & \mathbf{0} & \mathbf{0} \\ \mathbf{0} & \boldsymbol{S}_2^{-T}(A\boldsymbol{I}_\phi + J_\xi \boldsymbol{I}_{\phi'})\boldsymbol{S}_2^{-1} & \mathbf{0} \\ \mathbf{0} & \mathbf{0} & \boldsymbol{S}_3^{-T}J_p\boldsymbol{I}_\psi \boldsymbol{S}_3^{-1} \end{bmatrix} \in R^{10,10}, \tag{9}$$

$$\boldsymbol{K}_{AP}^{(e)} = \begin{bmatrix} \boldsymbol{S}_1^{-T}E^*J_\eta \boldsymbol{I}_{\phi''}\boldsymbol{S}_1^{-1} & \mathbf{0} & \mathbf{0} \\ \mathbf{0} & \boldsymbol{S}_2^{-T}E^*J_\xi \boldsymbol{I}_{\phi''}\boldsymbol{S}_2^{-1} & \mathbf{0} \\ \mathbf{0} & \mathbf{0} & \boldsymbol{S}_3^{-T}GJ_k \boldsymbol{I}_{\psi'}\boldsymbol{S}_3^{-1} \end{bmatrix} \in R^{10,10}, \tag{10}$$

where

$$\boldsymbol{I}_\chi = \int_0^l \boldsymbol{\chi}^T(x)\boldsymbol{\chi}(x)\mathrm{d}x, \ \boldsymbol{I}_{\chi'} = \int_0^l \boldsymbol{\chi}'^T(x)\boldsymbol{\chi}'(x)\mathrm{d}x, \ \boldsymbol{I}_{\chi''} = \int_0^l \boldsymbol{\chi}''^T(x)\boldsymbol{\chi}''(x)\mathrm{d}x, \ \boldsymbol{\chi} = \boldsymbol{\Phi}, \boldsymbol{\Psi};$$

$$\boldsymbol{S}_1 = \begin{bmatrix} 1 & 0 & 0 & 0 \\ 0 & 1 & 0 & 0 \\ 1 & l & l^2 & l^3 \\ 0 & 1 & 2l & 3l^2 \end{bmatrix}, \ \boldsymbol{S}_2 = \begin{bmatrix} 1 & 0 & 0 & 0 \\ 0 & -1 & 0 & 0 \\ 1 & l & l^2 & l^3 \\ 0 & -1 & -2l & -3l^2 \end{bmatrix}, \ \boldsymbol{S}_3 = \begin{bmatrix} 1 & 0 \\ 0 & l \end{bmatrix}$$

and $\boldsymbol{\Phi}(x) = [1, x, x^2, x^3]$, $\boldsymbol{\Psi}(x) = [1, x]$. Every beam element is determined by parameters ρ (mass density), A (cross-section area), J_ξ, J_η (second moment of the cross-section area to corresponding axes), J_p (polar second moment of area), $J_k \sim \frac{A^4}{40 J_p}$, l (length), E (Young's modulus), G (shear modulus) and $E^* = E\frac{1-\nu}{(1+\nu)(1-2\nu)}$ depends on Poisson's ratio ν.

To transform the model into general coordinates $\boldsymbol{q}_{AP,s}$ defined in (7) by mass and stiffness matrices must be transformed in the form

$$\boldsymbol{X}_e = \boldsymbol{P}^T \boldsymbol{X}^{(e)} \boldsymbol{P}, \ \boldsymbol{X} = \boldsymbol{M}, \boldsymbol{K}, \tag{11}$$

where

$$\boldsymbol{q}_{AP}^{(e)} = \boldsymbol{P}\widetilde{\boldsymbol{q}}_{AP}^{(e)}, \ \widetilde{\boldsymbol{q}}_{AP}^{(e)} = [\xi_{g-1}, \eta_{g-1}, \varphi_{g-1}, \vartheta_{g-1}, \psi_{g-1}, \xi_g, \eta_g, \varphi_g, \vartheta_g, \psi_g]^T.$$

Structure of the mass and stiffness matrices of one angle piece is given by following scheme

$$\boldsymbol{X}_{AP} = \sum_{e=1}^{G} \mathrm{diag}[\boldsymbol{0}, \boldsymbol{X}_e, \boldsymbol{0}], \ \boldsymbol{X} = \boldsymbol{M}, \boldsymbol{K} \tag{12}$$

with block matrices $\boldsymbol{X}_e$ determined in (11). Matrices of the first (lower) beam element in (12) must be arranged in accordance with angle pieces boundary conditions. The hardening of skeleton by welded grid rims within length l_{GR}, height h_{GR} and thickness t_{GR} (see Fig. 4) is respected by lateral beams fully restrained into adjacent angle pieces on the level of all spacer grids. The total mass and stiffness matrices of the skeleton in the coordinate system (6) have the form

$$\boldsymbol{M}_{LS} = \mathrm{diag}[\boldsymbol{M}_{AP} + \Delta\boldsymbol{M}_{GR}, \dots, \boldsymbol{M}_{AP} + \Delta\boldsymbol{M}_{GR}] \in R^{5GS},$$

$$\boldsymbol{K}_{LS} = \mathrm{diag}[\boldsymbol{K}_{AP}, \ldots, \boldsymbol{K}_{AP}] + \sum_{s=1}^{S} \sum_{g=1}^{G} \boldsymbol{K}_{GR,g}^{(s,s+1)} \in R^{5GS}, \tag{13}$$

where $\Delta \boldsymbol{M}_{GR}$ expresses additional mass matrix of the grid rims with mass concentrated into ends points of adjacent angle pieces on the level of all spacer grids and $\boldsymbol{K}_{GR,g}^{(s,s+1)}$ is stiffness matrix of one grid rim between adjacent angle pieces AP_s and AP_{s+1} on the level of spacer grid g.

3. Mathematical model of the fuel assembly

3.1. Structure of the fuel assembly model

The subsystems of FA are linked by spacer grids of different types for $g = 1$, $g = 2, \ldots, G - 1$ and $g = G$. In consequence of radial and orthogonal fuel rods and guide thimbles displacements mathematical models of segments are identical. Therefore the conservative model of the fuel assembly in configuration space

$$\boldsymbol{q} = [\boldsymbol{q}_1^T, \ldots, \boldsymbol{q}_s^T, \ldots, \boldsymbol{q}_S^T, \boldsymbol{q}_{CT}^T, \boldsymbol{q}_{LS}^T]^T \tag{14}$$

of dimension $n = 4GRS + 4G + 5GS$ can be written as

$$\boldsymbol{M}\ddot{\boldsymbol{q}} + (\boldsymbol{K} + \boldsymbol{K}_{S,S} + \boldsymbol{K}_{S,CT} + \boldsymbol{K}_{S,LS})\boldsymbol{q} = \boldsymbol{0}. \tag{15}$$

The mass $\boldsymbol{M}$ and stiffness $\boldsymbol{K}$ matrices correspond to a fictive fuel assembly divided into mutually uncoupled subsystems. Therefore these matrices are block diagonal

$$\boldsymbol{M} = \mathrm{diag}[\boldsymbol{M}_S, \ldots, \boldsymbol{M}_S, \boldsymbol{M}_{CT}, \boldsymbol{M}_{LS}], \ \boldsymbol{K} = \mathrm{diag}[\boldsymbol{K}_S^*, \ldots, \boldsymbol{K}_S^*, \boldsymbol{K}_{CT}, \boldsymbol{K}_{LS}], \tag{16}$$

where segment stiffness matrix $\boldsymbol{K}_S^*$ includes couplings between all fuel rods and guide thimbles inside the segment. According to equation (3) it holds $\boldsymbol{K}_S^* = \boldsymbol{K}_S + \sum_{q=1}^{Q} \sum_{g=1}^{G} \boldsymbol{K}_{q,g}$.

3.2. Modelling of couplings between FA subsystems

The stiffness matrix $\boldsymbol{K}_{i,j,g}^{(s,s+1)}$ of one coupling by spacer grid g between fuel rod i at segment s and fuel rod j at segment $s + 1$ has similar structure as matrix $\boldsymbol{K}_{q,g}$ in (3). Nonzero elements are localized at positions corresponding to displacements $\xi_{i,g}^{(s)}$, $\eta_{i,g}^{(s)}$ and $\xi_{j,g}^{(s+1)}$, $\eta_{j,g}^{(s+1)}$ in the vector of generalized coordinates $\boldsymbol{q}$ in (14). The total *coupling stiffness matrix between all segments* in the case of FA hexagonal type ($s = 1, \ldots, 6$) has structure

$$\boldsymbol{K}_{S,S} = \begin{bmatrix} \boldsymbol{K}_{1,1}^{S} & \boldsymbol{K}_{1,2}^{S} & 0 & 0 & 0 & \boldsymbol{K}_{1,6}^{S} & 0 & 0 \\ \boldsymbol{K}_{2,1}^{S} & \boldsymbol{K}_{2,2}^{S} & \boldsymbol{K}_{2,3}^{S} & 0 & 0 & 0 & 0 & 0 \\ 0 & \boldsymbol{K}_{3,2}^{S} & \boldsymbol{K}_{3,3}^{S} & \boldsymbol{K}_{3,4}^{S} & 0 & 0 & 0 & 0 \\ 0 & 0 & \boldsymbol{K}_{4,3}^{S} & \boldsymbol{K}_{4,4}^{S} & \boldsymbol{K}_{4,5}^{S} & 0 & 0 & 0 \\ 0 & 0 & 0 & \boldsymbol{K}_{5,4}^{S} & \boldsymbol{K}_{5,5}^{S} & \boldsymbol{K}_{5,6}^{S} & 0 & 0 \\ \boldsymbol{K}_{6,1}^{S} & 0 & 0 & 0 & \boldsymbol{K}_{6,5}^{S} & \boldsymbol{K}_{6,6}^{S} & 0 & 0 \\ 0 & 0 & 0 & 0 & 0 & 0 & 0 & 0 \\ 0 & 0 & 0 & 0 & 0 & 0 & 0 & 0 \end{bmatrix}. \tag{17}$$

Elastic properties of the spacer grids between the first fuel rods in all segments $s = 1, \ldots, S$ and the centre tube are expressed by stiffness $k_{S,CT}^{(g)}$ of the transverse springs on all level spacings $g = 1, \ldots, G$. The corresponding coupling stiffness matrix results from identity

$$\frac{\partial E_{S,CT}}{\partial \boldsymbol{q}} = \boldsymbol{K}_{S,CT} \boldsymbol{q} \,. \tag{18}$$

The potential (deformation) energy of these couplings is

$$E_{S,CT} = \sum_{s=1}^{S} \sum_{g=1}^{G} \frac{1}{2} k_{S,CT}^{(g)} (x_g \cos \alpha_s + y_g \sin \alpha_s - \xi_{1,g}^{(s)})^2 \,, \tag{19}$$

where in the case of hexagonal type of FA $\alpha_s = \frac{\pi}{6} + \frac{\pi}{3}(s-1)$ is radius vector angle of the first fuel rod in segment s with respect to x axis. The total *stiffness matrix between all segments and the centre tube* is

$$\boldsymbol{K}_{S,CT} = \sum_{s=1}^{S} \sum_{g=1}^{G} k_{S,CT}^{(g)} \begin{bmatrix} 1 & \cdots & -\cos \alpha_s & -\sin \alpha_s \\ \vdots & & \vdots & \vdots \\ -\cos \alpha_s & \cdots & \cos^2 \alpha_s & \sin \alpha_s \cos \alpha_s \\ -\sin \alpha_s & \cdots & \sin \alpha_s \cos \alpha_s & \sin^2 \alpha_s \end{bmatrix} \,, \tag{20}$$

where the introduced nonzero elements are localized at positions $4GR(s-1) + 4(g-1) + 1$ corresponding to fuel rod coordinates $\xi_{1,g}^{(s)}$ and $4GRS + 4(g-1) + 1 \div 2$ corresponding to centre tube coordinates x_g, y_g in the vector of generalized coordinates $\boldsymbol{q}$ in (14). This matrix for hexagonal type FA has structure

$$\boldsymbol{K}_{S,CT} = \begin{bmatrix} \boldsymbol{K}_{1,1}^{CT} & \boldsymbol{0} & \boldsymbol{0} & \boldsymbol{0} & \boldsymbol{0} & \boldsymbol{0} & \boldsymbol{K}_{1,CT} & \boldsymbol{0} \\ \boldsymbol{0} & \boldsymbol{K}_{2,2}^{CT} & \boldsymbol{0} & \boldsymbol{0} & \boldsymbol{0} & \boldsymbol{0} & \boldsymbol{K}_{2,CT} & \boldsymbol{0} \\ \boldsymbol{0} & \boldsymbol{0} & \boldsymbol{K}_{3,3}^{CT} & \boldsymbol{0} & \boldsymbol{0} & \boldsymbol{0} & \boldsymbol{K}_{3,CT} & \boldsymbol{0} \\ \boldsymbol{0} & \boldsymbol{0} & \boldsymbol{0} & \boldsymbol{K}_{4,4}^{CT} & \boldsymbol{0} & \boldsymbol{0} & \boldsymbol{K}_{4,CT} & \boldsymbol{0} \\ \boldsymbol{0} & \boldsymbol{0} & \boldsymbol{0} & \boldsymbol{0} & \boldsymbol{K}_{5,5}^{CT} & \boldsymbol{0} & \boldsymbol{K}_{5,CT} & \boldsymbol{0} \\ \boldsymbol{0} & \boldsymbol{0} & \boldsymbol{0} & \boldsymbol{0} & \boldsymbol{0} & \boldsymbol{K}_{6,6}^{CT} & \boldsymbol{K}_{6,CT} & \boldsymbol{0} \\ \boldsymbol{K}_{CT,1} & \boldsymbol{K}_{CT,2} & \boldsymbol{K}_{CT,3} & \boldsymbol{K}_{CT,4} & \boldsymbol{K}_{CT,5} & \boldsymbol{K}_{CT,6} & \boldsymbol{K}_{CT,CT} & \boldsymbol{0} \\ \boldsymbol{0} & \boldsymbol{0} & \boldsymbol{0} & \boldsymbol{0} & \boldsymbol{0} & \boldsymbol{0} & \boldsymbol{0} & \boldsymbol{0} \end{bmatrix} \,. \tag{21}$$

Every angle piece AP_s of the skeleton encircles fuel rods 10 and 19 of the segment s and fuel rod 55 of the segment $s-1$ (see Fig. 5). The potential (deformation) energy of one contact lateral springs $k_{S,AP}^{(g)}$ between single fuel rod r of the segment s and angle pieces AP_s on level spacings g is

$$E_{r,g}^{(s)} = \frac{1}{2} k_{S,AP}^{(g)} [\xi_{r,g}^{(s)} \cos(\delta - \alpha_r) + \eta_{r,g}^{(s)} \sin(\delta - \alpha_r) - \xi_{AP,g}^{(s)} \cos \delta - \eta_{AP,g}^{(s)} \sin \delta + e_r \varphi_{AP,g}^{(s)}]^2 \,. \tag{22}$$

The corresponding coupling stiffness matrix $\boldsymbol{K}_{r,g}^{(s)}$ results from identity

$$\frac{\partial E_{r,g}^{(s)}}{\partial \boldsymbol{q}} = \boldsymbol{K}_{r,g}^{(s)} \boldsymbol{q} \,, \tag{23}$$

whereas

$$\boldsymbol{K}_{r,g}^{(s)} = k_{S,AP}^{(g)} \begin{bmatrix} \vdots & \vdots & & \vdots & \vdots & \vdots & \\ \cdots & C^2 & SC & \cdots & -C\cos\delta & -C\sin\delta & e_r C & \cdots \\ \cdots & CS & S^2 & \cdots & -S\cos\delta & -S\sin\delta & e_r S & \cdots \\ & \vdots & \vdots & & \vdots & \vdots & \vdots & \\ \cdots & -C\cos\delta & -S\cos\delta & \cdots & \cos^2\delta & \sin\delta\cos\delta & -e_r\cos\delta & \cdots \\ \cdots & -C\sin\delta & -S\sin\delta & \cdots & \sin\delta\cos\delta & \sin^2\delta & -e_r\sin\delta & \cdots \\ \cdots & Ce_r & Se_r & \cdots & -e_r\cos\delta & -e_r\sin\delta & e_r^2 & \cdots \\ & \vdots & \vdots & & \vdots & \vdots & \vdots & \end{bmatrix} \quad (24)$$

and $C = \cos(\delta - \alpha_r)$, $S = \sin(\delta - \alpha_r)$. The introduced nonzero elements are localized at positions $4GR(s-1) + 4G(r-1) + 4(g-1) + 1 \div 2$ corresponding to fuel rod r coordinates $\xi_{r,g}^{(s)}$, $\eta_{r,g}^{(s)}$ and $4GRS + 4G + 5G(s-1) + 5(g-1) + 1 \div 3$ corresponding to angle piece AP_s coordinates $\xi_{AP,g}^{(s)}$, $\eta_{AP,g}^{(s)}$, $\varphi_{AP,g}^{(s)}$.
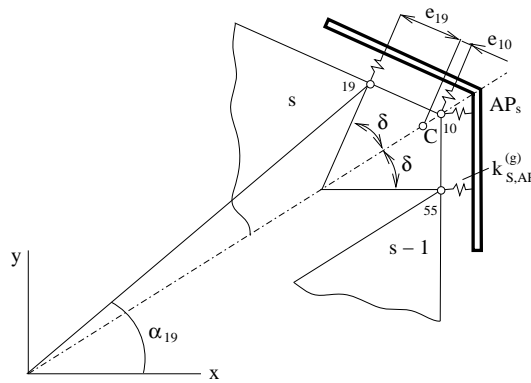

Fig. 5. Couplings between fuel rods of segments s and $s-1$ and the angle piece AP_s

The total stiffness matrix between fuel rods of all segments and all angle pieces (skeleton) is

$$\boldsymbol{K}_{S,LS} = \sum_{s=1}^{S} \sum_{g=1}^{G} \sum_{r=10,19,55} \boldsymbol{K}_{r,g}^{(s)}. \quad (25)$$

This matrix for hexagonal type FA has structure

$$\boldsymbol{K}_{S,LS} = \begin{bmatrix} \boldsymbol{K}_{1,1}^{LS} & 0 & 0 & 0 & 0 & 0 & 0 & \boldsymbol{K}_{1,LS} \\ 0 & \boldsymbol{K}_{2,2}^{LS} & 0 & 0 & 0 & 0 & 0 & \boldsymbol{K}_{2,LS} \\ 0 & 0 & \boldsymbol{K}_{3,3}^{LS} & 0 & 0 & 0 & 0 & \boldsymbol{K}_{3,LS} \\ 0 & 0 & 0 & \boldsymbol{K}_{4,4}^{LS} & 0 & 0 & 0 & \boldsymbol{K}_{4,LS} \\ 0 & 0 & 0 & 0 & \boldsymbol{K}_{5,5}^{LS} & 0 & 0 & \boldsymbol{K}_{5,LS} \\ 0 & 0 & 0 & 0 & 0 & \boldsymbol{K}_{6,6}^{LS} & 0 & \boldsymbol{K}_{6,LS} \\ 0 & 0 & 0 & 0 & 0 & 0 & 0 & 0 \\ \boldsymbol{K}_{LS,1} & \boldsymbol{K}_{LS,2} & \boldsymbol{K}_{LS,3} & \boldsymbol{K}_{LS,4} & \boldsymbol{K}_{LS,5} & \boldsymbol{K}_{LS,6} & 0 & \boldsymbol{K}_{LS,LS} \end{bmatrix}. \quad (26)$$

The coupling stiffness matrices $\boldsymbol{K}_{SS}$, $\boldsymbol{K}_{S,CT}$ and $\boldsymbol{K}_{S,LS}$ express interaction between appropriate subsystems marked in subscripts. Therefore nonzero submatrices correspond to mutually linked subsystems and zero submatrices express an absent of coupling between subsystems.

3.3. Condensed model of the fuel assembly

The FA model (15) has to large DOF number $n = 4GRS + 4G + 5GS$ for calculation of the dynamic response excited by different sources of excitation. Therefore it is necessary to compile the condensed FA model using the modal synthesis method [6]. The *first step* is the modal analysis of the mutually isolated subsystems presented in section two

$$\boldsymbol{M}_S\ddot{\boldsymbol{q}}_s + (\boldsymbol{K}_S + \sum_{q=1}^{Q}\sum_{g=1}^{G}\boldsymbol{K}_{q,g})\boldsymbol{q}_s = \boldsymbol{0} \implies \boldsymbol{\Lambda}_S,\, \boldsymbol{V}_S \in R^{n_S},\, n_S = 4GR,$$

$$\boldsymbol{M}_{CT}\ddot{\boldsymbol{q}}_{CT} + \boldsymbol{K}_{CT}\boldsymbol{q}_{CT} = \boldsymbol{0} \implies \boldsymbol{\Lambda}_{CT},\, \boldsymbol{V}_{CT} \in R^{n_{CT}},\, n_{CT} = 4G,\qquad(27)$$

$$\boldsymbol{M}_{LS}\ddot{\boldsymbol{q}}_{LS} + \boldsymbol{K}_{LS}\boldsymbol{q}_{LS} = \boldsymbol{0} \implies \boldsymbol{\Lambda}_{LS},\, \boldsymbol{V}_{LS} \in R^{n_{LS}},\, n_{LS} = 5GS,$$

where $\boldsymbol{\Lambda}_X$, $\boldsymbol{V}_X$, $X = S, CT, LS$ are spectral and modal matrices of the subsystems, fulfilling the orthonormality conditions $\boldsymbol{V}_X^T\boldsymbol{M}_X\boldsymbol{V}_X = \boldsymbol{E}$, $\boldsymbol{V}_X^T\boldsymbol{K}_X\boldsymbol{V}_X = \boldsymbol{\Lambda}_X$. Further we choose a set of m_S low-frequency eigenvectors of the rod segment which will be arranged in its modal submatrix ${}^m\boldsymbol{V}_S \in R^{n_S,m_S}$ corresponding to spectral submatrix ${}^m\boldsymbol{\Lambda}_S \in R^{m_S,m_S}$. A set of other rod segment eigenmodes of each segment will be neglected. The *second step* is the transformation of the global vector of generalized coordinates defined in (14) by means of modal matrices (submatrices) of subsystems in the form

$$\boldsymbol{q} = \begin{bmatrix} \boldsymbol{q}_1 \\ \boldsymbol{q}_2 \\ \vdots \\ \boldsymbol{q}_S \\ \boldsymbol{q}_{CT} \\ \boldsymbol{q}_{LS} \end{bmatrix} = \begin{bmatrix} {}^m\boldsymbol{V}_S & \boldsymbol{0} & \dots & \boldsymbol{0} & \boldsymbol{0} & \boldsymbol{0} \\ \boldsymbol{0} & {}^m\boldsymbol{V}_S & \dots & \boldsymbol{0} & \boldsymbol{0} & \boldsymbol{0} \\ \dots & & & & & \\ \boldsymbol{0} & \boldsymbol{0} & \dots & {}^m\boldsymbol{V}_S & \boldsymbol{0} & \boldsymbol{0} \\ \boldsymbol{0} & \boldsymbol{0} & \dots & \boldsymbol{0} & \boldsymbol{V}_{CT} & \boldsymbol{0} \\ \boldsymbol{0} & \boldsymbol{0} & \dots & \boldsymbol{0} & \boldsymbol{0} & \boldsymbol{V}_{LS} \end{bmatrix} \begin{bmatrix} \boldsymbol{x}_1 \\ \boldsymbol{x}_2 \\ \vdots \\ \boldsymbol{x}_S \\ \boldsymbol{x}_{CT} \\ \boldsymbol{x}_{LS} \end{bmatrix}\qquad(28)$$

for short

$$\boldsymbol{q} = {}^m\boldsymbol{V}\boldsymbol{x},\ {}^m\boldsymbol{V} \in R^{n,m},\ m = Sm_S + 4G + 5GS.\qquad(29)$$

The stiffness matrix of all couplings between subsystems is

$$\boldsymbol{K}_C = \boldsymbol{K}_{S,S} + \boldsymbol{K}_{S,CT} + \boldsymbol{K}_{S,LS}\qquad(30)$$

and according to (17), (21) and (26) for hexagonal type FA ($S = 6$) has block structure

$$\boldsymbol{K}_C = \begin{bmatrix} \boldsymbol{K}_{1,1} & \boldsymbol{K}_{1,2}^S & \boldsymbol{0} & \boldsymbol{0} & \boldsymbol{0} & \boldsymbol{K}_{1,6}^S & \boldsymbol{K}_{1,CT} & \boldsymbol{K}_{1,LS} \\ \boldsymbol{K}_{2,1}^S & \boldsymbol{K}_{2,2} & \boldsymbol{K}_{2,3}^S & \boldsymbol{0} & \boldsymbol{0} & \boldsymbol{0} & \boldsymbol{K}_{2,CT} & \boldsymbol{K}_{2,LS} \\ \boldsymbol{0} & \boldsymbol{K}_{3,2}^S & \boldsymbol{K}_{3,3} & \boldsymbol{K}_{3,4}^S & \boldsymbol{0} & \boldsymbol{0} & \boldsymbol{K}_{3,CT} & \boldsymbol{K}_{3,LS} \\ \boldsymbol{0} & \boldsymbol{0} & \boldsymbol{K}_{4,3}^S & \boldsymbol{K}_{4,4} & \boldsymbol{K}_{4,5}^S & \boldsymbol{0} & \boldsymbol{K}_{4,CT} & \boldsymbol{K}_{4,LS} \\ \boldsymbol{0} & \boldsymbol{0} & \boldsymbol{0} & \boldsymbol{K}_{5,4}^S & \boldsymbol{K}_{5,5} & \boldsymbol{K}_{5,6}^S & \boldsymbol{K}_{5,CT} & \boldsymbol{K}_{5,LS} \\ \boldsymbol{K}_{6,1}^S & \boldsymbol{0} & \boldsymbol{0} & \boldsymbol{0} & \boldsymbol{K}_{6,5}^S & \boldsymbol{K}_{6,6} & \boldsymbol{K}_{6,CT} & \boldsymbol{K}_{6,LS} \\ \boldsymbol{K}_{CT,1} & \boldsymbol{K}_{CT,2} & \boldsymbol{K}_{CT,3} & \boldsymbol{K}_{CT,4} & \boldsymbol{K}_{CT,5} & \boldsymbol{K}_{CT,6} & \boldsymbol{K}_{CT,CT} & \boldsymbol{0} \\ \boldsymbol{K}_{LS,1} & \boldsymbol{K}_{LS,2} & \boldsymbol{K}_{LS,3} & \boldsymbol{K}_{LS,4} & \boldsymbol{K}_{LS,5} & \boldsymbol{K}_{LS,6} & \boldsymbol{0} & \boldsymbol{K}_{LS,LS} \end{bmatrix}.\qquad(31)$$

The diagonal block matrices are

$$\boldsymbol{K}_{i,i} = \boldsymbol{K}_{i,i}^S + \boldsymbol{K}_{i,i}^{CT} + \boldsymbol{K}_{i,i}^{LS},\ i = 1,\dots,6.$$

After the transformation (29) applied to FA model (15) the FA condensed conservative model

$$\ddot{\boldsymbol{x}} + ({}^m\boldsymbol{\Lambda} + {}^m\boldsymbol{V}^T\boldsymbol{K}_C\,{}^m\boldsymbol{V})\boldsymbol{x} = \boldsymbol{0} \tag{32}$$

has $m = Sm_S + 4G + 5GS$ DOF number. Matrices of the condensed model have the block structure corresponding to FA decomposition

$$^m\boldsymbol{\Lambda} = \mathrm{diag}[{}^m\boldsymbol{\Lambda}_S, \ldots, {}^m\boldsymbol{\Lambda}_S, \boldsymbol{\Lambda}_{CT}, \boldsymbol{\Lambda}_{LS}] \in R^{m,m} \tag{33}$$

and

$$^m\boldsymbol{V}^T\boldsymbol{K}_C\,{}^m\boldsymbol{V} = \begin{bmatrix} \widetilde{\boldsymbol{K}}_{1,1} & \widetilde{\boldsymbol{K}}_{1,2} & \boldsymbol{0} & \boldsymbol{0} & \boldsymbol{0} & \widetilde{\boldsymbol{K}}_{1,6} & \widetilde{\boldsymbol{K}}_{1,CT} & \widetilde{\boldsymbol{K}}_{1,LS} \\ \widetilde{\boldsymbol{K}}_{2,1} & \widetilde{\boldsymbol{K}}_{2,2} & \widetilde{\boldsymbol{K}}_{2,3} & \boldsymbol{0} & \boldsymbol{0} & \boldsymbol{0} & \widetilde{\boldsymbol{K}}_{2,CT} & \widetilde{\boldsymbol{K}}_{2,LS} \\ \boldsymbol{0} & \widetilde{\boldsymbol{K}}_{3,2} & \widetilde{\boldsymbol{K}}_{3,3} & \widetilde{\boldsymbol{K}}_{3,4} & \boldsymbol{0} & \boldsymbol{0} & \widetilde{\boldsymbol{K}}_{3,CT} & \widetilde{\boldsymbol{K}}_{3,LS} \\ \boldsymbol{0} & \boldsymbol{0} & \widetilde{\boldsymbol{K}}_{4,3} & \widetilde{\boldsymbol{K}}_{4,4} & \widetilde{\boldsymbol{K}}_{4,5} & \boldsymbol{0} & \widetilde{\boldsymbol{K}}_{4,CT} & \widetilde{\boldsymbol{K}}_{4,LS} \\ \boldsymbol{0} & \boldsymbol{0} & \boldsymbol{0} & \widetilde{\boldsymbol{K}}_{5,4} & \widetilde{\boldsymbol{K}}_{5,5} & \widetilde{\boldsymbol{K}}_{5,6} & \widetilde{\boldsymbol{K}}_{5,CT} & \widetilde{\boldsymbol{K}}_{5,LS} \\ \widetilde{\boldsymbol{K}}_{6,1} & \boldsymbol{0} & \boldsymbol{0} & \boldsymbol{0} & \widetilde{\boldsymbol{K}}_{6,5} & \widetilde{\boldsymbol{K}}_{6,6} & \widetilde{\boldsymbol{K}}_{6,CT} & \widetilde{\boldsymbol{K}}_{6,LS} \\ \widetilde{\boldsymbol{K}}_{CT,1} & \widetilde{\boldsymbol{K}}_{CT,2} & \widetilde{\boldsymbol{K}}_{CT,3} & \widetilde{\boldsymbol{K}}_{CT,4} & \widetilde{\boldsymbol{K}}_{CT,5} & \widetilde{\boldsymbol{K}}_{CT,6} & \widetilde{\boldsymbol{K}}_{CT} & \boldsymbol{0} \\ \widetilde{\boldsymbol{K}}_{LS,1} & \widetilde{\boldsymbol{K}}_{LS,2} & \widetilde{\boldsymbol{K}}_{LS,3} & \widetilde{\boldsymbol{K}}_{LS,4} & \widetilde{\boldsymbol{K}}_{LS,5} & \widetilde{\boldsymbol{K}}_{LS,6} & \boldsymbol{0} & \widetilde{\boldsymbol{K}}_{LS} \end{bmatrix}, \tag{34}$$

where

$$\widetilde{\boldsymbol{K}}_{i,j} = {}^m\boldsymbol{V}_S^T\boldsymbol{K}_{i,j}\,{}^m\boldsymbol{V}_S\,;\ \ \widetilde{\boldsymbol{K}}_{i,CT} = {}^m\boldsymbol{V}_S^T\boldsymbol{K}_{i,CT}\boldsymbol{V}_{CT}\,;\ \ \widetilde{\boldsymbol{K}}_{i,LS} = {}^m\boldsymbol{V}_S^T\boldsymbol{K}_{i,LS}\boldsymbol{V}_{LS}\,;$$

$$\widetilde{\boldsymbol{K}}_{CT,j} = \boldsymbol{V}_{CT}^T\boldsymbol{K}_{CT,j}\,{}^m\boldsymbol{V}_S\,;\ \ \widetilde{\boldsymbol{K}}_{LS,j} = \boldsymbol{V}_{LS}^T\boldsymbol{K}_{LS,j}\,{}^m\boldsymbol{V}_S\,;\ \ \widetilde{\boldsymbol{K}}_{CT} = \boldsymbol{V}_{CT}^T\boldsymbol{K}_{CT,CT}\boldsymbol{V}_{CT}\,;$$

$$\widetilde{\boldsymbol{K}}_{LS} = \boldsymbol{V}_{LS}^T\boldsymbol{K}_{LS,LS}\boldsymbol{V}_{LS}\,;\ \ i = 1, \ldots, 6\,;\ \ j = 1, \ldots, 6\,.$$

Eigenfrequencies Ω_ν and eigenvectors

$$\boldsymbol{x}_\nu = [\boldsymbol{x}_{1,\nu}^T, \ldots, \boldsymbol{x}_{S,\nu}^T, \boldsymbol{x}_{CT,\nu}^T, \boldsymbol{x}_{LS,\nu}^T]^T,\ \nu = 1, \ldots, m$$

of FA are obtained from the modal analysis of the condensed model (32). Subvectors $\boldsymbol{x}_{s,\nu}$ ($s = 1, \ldots, S$) corresponding to rod segments, $\boldsymbol{x}_{CT,\nu}$ to centre tube and $\boldsymbol{x}_{LS,\nu}$ to skeleton, can be transformed according to (28) from the space of coordinates of the condensed model (32) to the original configuration space of the generalized coordinates ob subsystems by

$$\boldsymbol{q}_{X,\nu} = {}^m\boldsymbol{V}_X\boldsymbol{x}_{X,\nu},\ X = 1, \ldots, S, CT, LS\,.$$

The eigenvalues calculated using condensed model (32) must be checked in light of accuracy with respect to noncondensed model (15) for different number m_S of applied rod segment master eigenvectors on the basis of the cumulative relative error of the eigenfrequencies and the normalized cross orthogonality matrix [11].

4. Application

The presented methodology and developed software in Matlab code was tested for the Russian TVSA-T fuel assembly used in nuclear power plant Temelín [8]. This FA of the hexagonal type (Fig. 1 and Fig. 2) has six rod segments ($S = 6$) and eight spacer grids ($G = 8$). Each segment contains 52 fuel rods and 3 guide thimbles ($R = 55$) linked by 135 transverse springs between

adjacent rods within stiffnesses $k_1 = 2 \cdot 10^5$, $k_2 = \cdots = k_7 = 1,83 \cdot 10^5$, $k_8 = 2,07 \cdot 10^5$ N/m on particular levels of spacer grids $g = 1, \ldots, 8$. The rod spacing is 12.75 mm. The noncondensed FA model under consideration has $n = 10\,832\,(n_S = 1\,760, n_{CT} = 32, n_{LS} = 240)$ DOF number. The lowest FA eigenfrequencies are $f_1 = f_2 = 3.43$ Hz at temperature $20\,°C$ and $f_1 = f_2 = 3.09$ Hz at temperature $350\,°C$. Pairs of eigenfrequencies correspond to flexural and breathing mode shapes and single eigenfrequencies correspond to torsion mode shapes. The spectrum of nineteen lowest (up to 20 Hz) eigenfrequencies with the characteristics of corresponding mode shapes is presented in Table 1. For the sake of completeness we introduce measured flexural mode shapes at temperature $20\,°C$ provided by ŠKODA, Nuclear Machinery, Co.Ltd.

Table 1. Eigenfrequencies and characteristics of corresponding natural modes of the FA model

ν	Eigenfrequencies [Hz]			Characteristics of mode shapes
	$t = 350^o$	$t = 20^o$	Measured	
1	3.09	3.43	3.9	Flexural, 1.mode
2	3.09	3.43		
3	4.13	4.58		Torsional, 1. mode
4	6.24	6.90	6.6	Flexural, 2. mode
5	6.24	6.90		
6	8.71	9.46		Torsional, 2. mode
7	9.49	10.46	9.4	Flexural, 3. mode
8	9.49	10.46		
9	11.74	12.56		Torsional, 3. mode
10	12.88	14.21	12.5	Flexural, 4. mode
11	12.88	14.21		
12	14.24	15.22		Torsional, 4. mode
13	16.47	18.17	18.6	Flexural, 5. mode
14	16.47	18.17		
15	17.23	18.60		Torsional, 5. mode
16	19.26	19.33		Breathing mode
17	19.26	19.33		
18	19.79	19.98		Breathing mode
19	19.79	19.98		

The spectrum of eigenfrequencies is very crowded especially for higher frequencies. The flexural mode shapes (Fig. 6,7) are characterized by inphase deformations of all FA components whereas spacer grids are practically non-deformed. The torsional mode shapes are characterized by maximal deformations of outsider fuel rods (Fig. 8) and spacer grids roll up practically without their deformations. The breathing modes (Fig. 9, 10) corresponding to higher eigenfrequencies approximately from 20 Hz (see Table 1) are characterized by spacer grid deformations and relatively high contact forces between fuel rods and spacer grids. All mode shapes in Fig. 6–10 are vizualized on the FA cross-section on the level of the fourth (central) spacer grid.
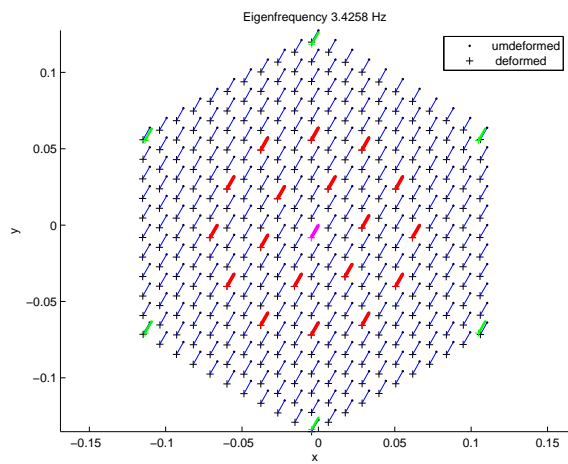
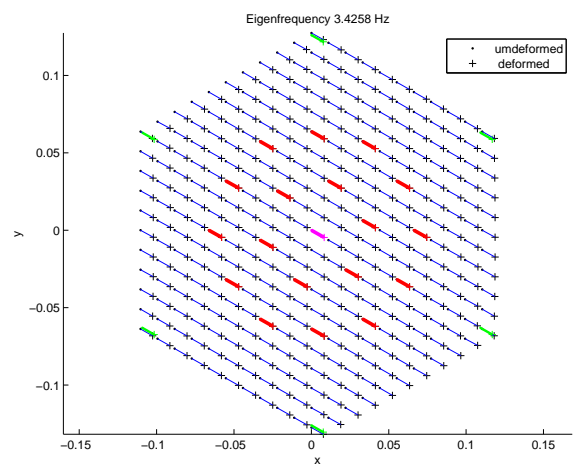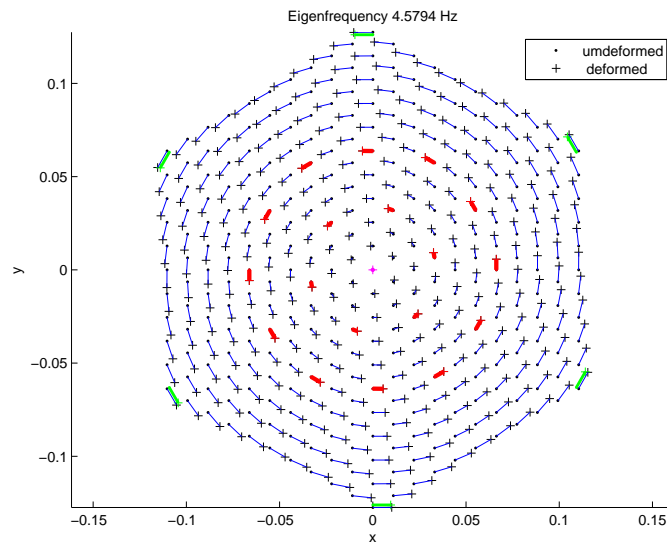Fig. 6. The first FA mode shape (flexural mode)   Fig. 7. The second FA mode shape (flexural mode)
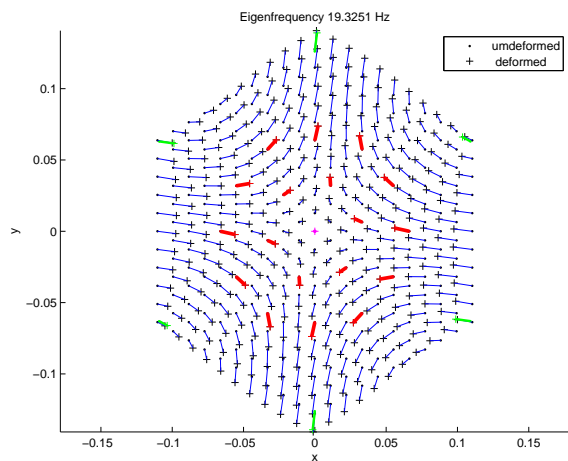

Fig. 8. The third FA mode shape (torsional mode)
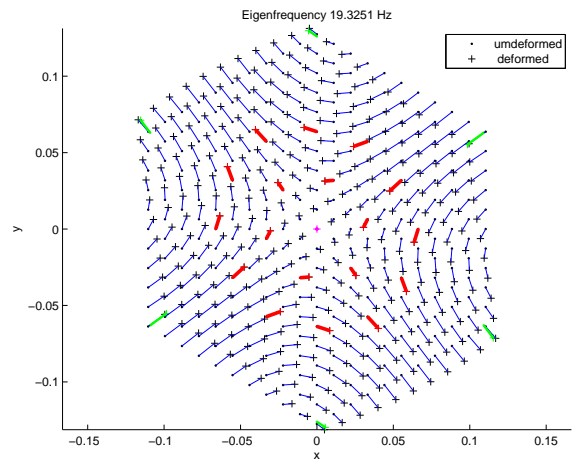

Fig. 9. The 16th FA mode shape (breathing mode)   Fig. 10. The 17th FA mode shape (breathing mode)

5. Conclusion

The described method enables to model effectively the flexural and torsional vibration of nuclear fuel assemblies. The special coordinate system of radial and orthogonal displacements of the fuel assembly components — fuel rods, guide thimbles, centre tube and skeleton angle pieces — enables to separate the system into several identical revolved rod segments characterized by identical mass and stiffness matrices, centre tube and load-bearing skeleton as subsystems. The subsystems are linked by spacer grids of different types on particular levels of spacer grids.

This new approach to modelling based on the system decomposition enables simple including of model particular components with identified parameters into global FA model, to significantly decrease of time demands of computing program assembladge and to save the computer memory. The preliminary results of the modal analysis of the Russian TVSA-T fuel assembly show, that in low-frequency spectrum of excitation (approximately up to 20 Hz) the flexural and torsional mode shapes are employed and in high-frequency spectrum the breathing mode shapes, characterized by spacer grid deformation on all levels, are employed.

The condensed FA model based on modal synthesis method with reduction of rod segment DOF number, will be applied to calculation of forced vibration caused by pressure pulsations and seismic excitation in terms of fuel assembly component deformations and abrasion of fuel rods coating.

Acknowledgements

References

[1] Byrtus, M., Hajžman, M., Zeman, V., Dynamics of rotating systems, University of West Bohemia, Plzeň, 2010 (in Czech).

[2] Hlaváč, Z., Zeman, V., The seismic response affection of the nuclear reactor WWER1000 by nuclear fuel assemblies, Engineering Mechanics, 3/4 (17) (2010) 147–160.

[3] Hlaváč, Z., Zeman, V., Flexural vibration of the package of rods linked by lattices, Proceedings of the 8-th conference Dynamic of rigid and deformable bodies 2010, Ústí nad Labem, 2010 (in Czech).

[4] Lavreňuk, P. I., Obosnovanije sovmestnosti TVSA-T PS CUZ i SVP s projektom AES Temelín, Statement from technical report TEM-GN-01, Sobstvennost' OAO TVEL (inside information of NRI Řež, 2009).

[5] Pečínka, L., Criterion assessment of fuel assemblies behaviour VV6 and TVSA-T at standard operating conditions of ETE V1000/320 type reactor, Research report DITI 300/406, NRIŘež, 2009 (in Czech).

[6] Slavík, J., Stejskal, V., Zeman, V., Elements of dynamics of machines, ČVUT, Praha, 1997 (in Czech).

[7] Smolík, J., and coll., Vvantage 6 Fuel Assembly Mechanical Test, Technical Report No. Ae 18018T, Škoda, Nuclear Machinery, Pilsen, Co.Ltd., 1995.

[8] Sýkora, M., Reactor TVSA-T fuel assembly insertion, part 4, Research report Pp BZ1, 2, ČEZ-ETE, 2009 (in Czech).

[9] Zeman, V., Hlaváč, Z., Modelling of WWER 1000 type reactor by means of decomposition method, Engineering Mechanics 2006, Institute of Theoretical and Applied Mechanics AS CR, Prague 2006, p. 444 (full paper on CD-ROM in Czech).

[10] Zeman, V., Hlaváč, Z., Dynamic response of VVER 1000 type reactor excited by pressure pulsations, Engineering Mechanics 6 (15) (2008) 435–446.

[11] Zeman, V., Hlaváč, Z., Modal properties of the flexural vibrating package of rods linked by spacer grids, Applied and Computational Mechanics 1 (5) (2011) 111–122.